$\mathcal{E}_m$. Spielman *et al.*[12] observed a similar bandwidth effect on T_h. However, the most striking and important effect appears to be the reduction in $\mathcal{E}_m$ observed in our experiment and predicted theoretically.

The total number of hot electrons also decreases as the bandwidth is increased ($n_h \propto (\Delta\omega/\omega_0)^{-0.43}$). One would not expect finite bandwidth to affect the amount of energy deposited through resonance absorption on the basis of the cold-plasma model. However, we find experimentally considerable reductions in profile modifications (2.7% vs 14%) which could in turn change the total absorption.

In conclusion, we have shown that at low power levels the cold-plasma wave-breaking model accurately predicts the wave-breaking time t_b, scaling of the electric field E_b, and maximum wave-breaking energy $\mathcal{E}_m$. Furthermore, the hot-electron temperature T_h scales with $\mathcal{E}_m$. The transition from convective saturation to wave-breaking saturation was found to occur when $v_{wave} \simeq v_{te}$. Finally, we have shown that finite pump bandwidth reduces the hot-electron temperature, increases the wave-breaking time, and decreases the field amplitude and maximum electron energy as predicted.

This work was supported by U. S. Department of Energy Contract No. DE-AS08-81 DP40143 and by the U. S. Air Force Office of Scientific Research Contract No. F49620-76-C-0012.

[a]Permanent address: Faculty of Engineering, Utsunomiya University, Utsunomiya, Japan.
[b]Permanent address: Naval Research Laboratory, Washington, D. C. 20375.
[1]V. L. Ginsburg, *The Properties of Electromagnetic Waves in Plasmas* (Pergamon, New York, 1964).
[2]D. W. Forslund, J. M. Kindel, and K. Lee, Phys. Rev. Lett. 39, 284 (1977).
[3]K. Estabrook and W. L. Kruer, Phys. Rev. Lett. 40, 42 (1978).
[4]J. R. Albritton and A. B. Langdon, Phys. Rev. Lett. 45, 1794 (1980).
[5]E. A. Williams and J. R. Albritton, in Proceedings of the Ninth Annual Conference on Anomalous Absorption of Electromagnetic Waves, Rochester, N. Y., 15–18 May 1979 (unpublished), paper C-2.
[6]B. Bezzerides, S. J. Gitomer, and D. W. Forslund, Phys. Rev. Lett. 44, 651 (1980).
[7]P. Koch and J. Albritton, Phys. Rev. Lett. 32, 1420 (1974).
[8]S. P. Obenschain and N. C. Luhmann, Jr., Phys. Rev. Lett. 42, 311 (1979).
[9]S. P. Obenschain, N. C. Luhmann, Jr., and P. T. Greiling, Phys. Rev. Lett. 36, 1309 (1976).
[10]S. P. Obenschain and N. C. Luhmann, Jr., Appl. Phys. Lett. 30, 452 (1977).
[11]K. G. Estabrook, E. J. Valeo, and W. L. Kruer, Phys. Fluids 18, 1151 (1975).
[12]R. B. Spielman, W. M. Bollen, K. Mizuno, and J. S. DeGroot, Phys. Rev. Lett. 46, 821 (1981).

Class of Model Stellarator Fields with Enhanced Confinement

H. E. Mynick,[a] T. K. Chu, and A. H. Boozer
Princeton Plasma Physics Laboratory, Princeton University, Princeton, New Jersey 08544
(Received 6 July 1981)

A class of model stellarator fields has been found in which the transport is reduced by an order of magnitude from transport in conventional stellarators, by localizing the helical ripple to the inside of the torus. The reduction is observed in numerical experiments, and explained theoretically. Realizations of this class are achievable with use of modular coils.

PACS numbers: 52.55.Gb

We report here on the discovery of a family of model stellarator configurations having transport which is greatly reduced from that which has been theoretically predicted,[1,2] and observed in numerical experiments,[3] for the standard configuration traditionally envisioned. Such an enhancement of confinement is important, since the transport levels predicted by the theory of Refs. 1 and 2 may be too large to make a stellarator reactor of acceptable size.

The new configurations are related to one proposed by Meyer and Schmidt[4] (the MS configuration). There, the objective was to improve the equilibrium properties at high β (the ratio of the pressures of the plasma and the confining magnetic field) by reducing the Pfirsch-Schluter currents J_{PS}. This is achieved by localizing the ripple in the magnetic field $\vec{B}$ induced by the helical

windings to the inside of the torus (poloidal angle θ near π), in such a way that the Fourier component of $B \equiv |\vec{B}|$ at $\cos\theta$, which gives rise to J_{PS}, is approximately eliminated. The present class of stellarators shares with the MS configuration the localization of the helical ripple to the inside of the torus. However, here the $\cos\theta$ component of B must *not* be eliminated; its optimum size will be discussed later in this paper.

Realizations of the configuration are obtainable with use of modular coils, and members of this class have been found[5] which possess a minimum average-B magnetic well. One may thus expect such configurations to possess good magnetohydrodynamic stability properties.

Numerical results for stellarator transport have previously been obtained showing slightly better[6] or dramatically better[7] confinement at low collision frequency ν than that predicted theoretically. However, the origin of this improved confinement was not understood. In Ref. 3 (where the theoretical predictions were *confirmed* numerically), it was argued that, while one might question aspects of the numerical and statistical procedures in Ref. 7, part of the explanation for the very favorable numerical results obtained there could lie in the richer harmonic content of $B(r;\varphi,\theta)$ over a flux surface (r = const). The configurations investigated here are one example of the improvement of transport through a more complex structure of B, and the physical mechanism for the improvement is described here.

We adopt a coordinate system natural to the magnetic geometry. We use the flux function ψ as the radial coordinate, satisfying $\vec{B}\cdot\nabla\psi = 0$, or equivalently, a radial variable $r(\psi)$ having units of length, defined by $\psi = \frac{1}{2}B_0 r^2$, with B_0 the toroidal field strength on the magnetic axis. Each ψ surface is parametrized by poloidal angle θ and toroidal angle φ, chosen so that the rotational transform $q^{-1} \equiv d\theta/d\varphi$ of a field line is a function of ψ only. The guiding-center equations of motion in these coordinates are then given, once a description for field strength $B(r,\varphi,\theta)$ is specified.[6] We compare three configurations here, designated by configuration index $\sigma = 0, \pm 1$, given for all r by

$$B(r,\varphi,\theta) = B_0[1 - \epsilon_t\cos\theta - \epsilon_h\cos\eta + \tfrac{1}{2}\sigma(\epsilon_{h-}\cos\eta_- + \epsilon_{h+}\cos\eta_+)]. \quad (1)$$

Here $\eta \equiv l\theta - m\varphi$, $\eta_\pm \equiv l_\pm\theta - m\varphi$, $l_\pm \equiv l \pm 1$, $\epsilon_h(r) \propto r^l$, $\epsilon_{h\pm}(r) \propto r^{l_\pm}$, $\epsilon_t(r) \equiv r/R_0 \equiv \epsilon_a r/a$ is the inverse aspect ratio, and a is the value of r at the plasma edge. The standard configuration of Refs. 1–3 is given by $\sigma = 0$. In the present configuration, at a particular value r_1 of r, $\epsilon_{h\pm}$ are chosen to satisfy $\epsilon_h(r_1) = \epsilon_{h+}(r_1) = \epsilon_{h-}(r_1)$. Then Eq. (1) takes the simpler form

$$B(r,\varphi,\theta) = B_0[1 - \epsilon_t\cos\theta - \epsilon_h\cos\eta(1 - \sigma\cos\theta)], \quad (2)$$

where the modulating envelope $(1 - \sigma\cos\theta)$ localizes the ripple to the interior (exterior) of the torus, for $\sigma = 1$ (-1). The $\sigma = 1$ configuration is the one with improved confinement; the -1 configuration has poorer confinement, and is studied to help discern the physical origin of the improvement for $\sigma = 1$.

In Figs. 1(a)–1(c) are shown profiles of B along a field line for $\sigma = 0$, 1, and -1, respectively, for $l = 2$, $m = 6$, $q^{-1} = 0.3$, $\epsilon_t = 0.05$, and $\epsilon_h = \epsilon_{h+} = \epsilon_{h-} = 0.05$ at $r_1/a = 0.5$. The flat-bottomed appearance of the $\sigma = 1$ B envelope is the result of the particular choice $p \equiv \epsilon_h/\epsilon_t = 1$ we take for the transport results shown here; this is not a necessary, nor even optimal, value for p.

In the numerical results to be presented shortly, the $\sigma = 1$ configuration shows much better confinement than the $\sigma = 0$ or -1 configuration. The most important reason for this is that, for almost all helically trapped particles, the contribution to the radial drift $\dot{r}$ coming from the $(1 - \cos\theta)$ modulation of ϵ_h *cancels* the toroidal contribution [cf. Eq. (3)]. This configuration thus has drifts which can approach being omnigenous[8] (i.e., having $\dot{r} = 0$), for the most troublesome particles in the $\sigma = 0$ configuration.

For these particles, the drifts normal to $\hat{B}$

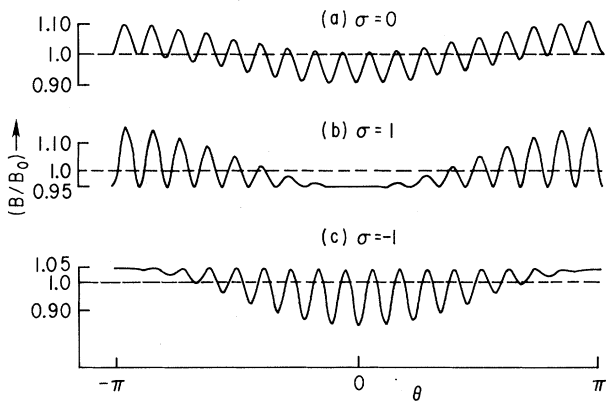

FIG. 1. Profiles of magnetic field strength along a field line for the three configurations studied.

$\equiv \vec{B}/B$ are dominated by the grad-B drift $\vec{v}_B = (\mu/m\Omega)\hat{B}\times\nabla B$, where $\mu \equiv m v_\perp^2/2B$ is the particle's magnetic moment, and $\Omega \equiv eB/mc$ is its gyrofrequency. (Here and throughout, we assume that there are no electric fields, which may also have a beneficial effect on confinement.) Assuming $\hat{B} \simeq \hat{\varphi}$, using Eq. (1) near $r = r_1$ to compute ∇B, and averaging over a helical bounce period τ_b, we obtain the drifts in the r and θ directions:

$$\dot{r} = v_{Bt}\sin\theta(1 - \sigma p\langle\cos\eta\rangle), \tag{3}$$

$$\Omega_\theta \equiv \dot{\theta} = v_{Bt}[\cos\theta + lp(1 - \sigma\cos\theta)\langle\cos\eta\rangle]/r. \tag{4}$$

Here $v_{Bt} \equiv \mu\epsilon_t B_0/m\Omega r$ is the toroidal contribution to v_B, and the angular brackets denote an average over τ_b. For $\sigma = \pm 1$, one sees from Eq. (3) that the radial drifts are modified, as a result of the $(1 - \sigma\cos\theta)$ modulation of ϵ_h.

For $\sigma p\langle\cos\eta\rangle = 1$, the drifts are fully omnigenous. The function $\langle\cos\eta(x)\rangle$ is plotted in Fig. 2 as a function of particle depth $x \equiv (E_{\parallel b}/E_{\parallel \max})^{1/2}$ in a helical well. (Here $E_{\parallel b}$ is the parallel energy of a particle at the well bottom, and $E_{\parallel\max}$ is the maximum $E_\parallel$ a trapped particle can have in that well.) For deeply trapped particles ($x \simeq 0$), $\langle\cos\eta\rangle$ is near 1, and for all but the most shallowly trapped, $\langle\cos\eta\rangle$ is positive, causing a reduction in $\dot{r}$ for $\sigma = 1$, and an enhancement for $\sigma = -1$. In order to optimize confinement, one wants $\dot{r}$ for a typical trapped particle to be zero. One would thus expect a value of $p = \epsilon_h/\epsilon_t$ somewhat greater than unity to be optimal.

The effect of this on particle orbits is illustrated by Figs. 3(a) and 3(b). These are poloidal projections of typical dominant contributors to the transport for their respective particle ensembles, for $\sigma = 1$ [Fig. 3(a)] and $\sigma = -1$ [Fig. 3(b)], at an initial radius for which $p \simeq 1$. After the initial helical entrapment at point A in Fig. 3(a), the particle takes a fairly rapid radial step Δr_b, until it becomes deeply enough trapped to largely shut off $\dot{r}$. Thereafter, the drift motion is almost at constant r.

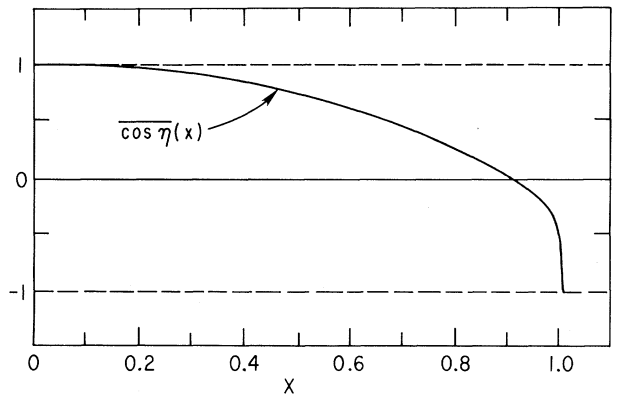

FIG. 2. Plot of the bounce-averaged value of $\cos\eta$ as a function of well-depth parameter x. Particles trapped at the well bottom have $x = 0$; those barely trapped have $x = 1$.

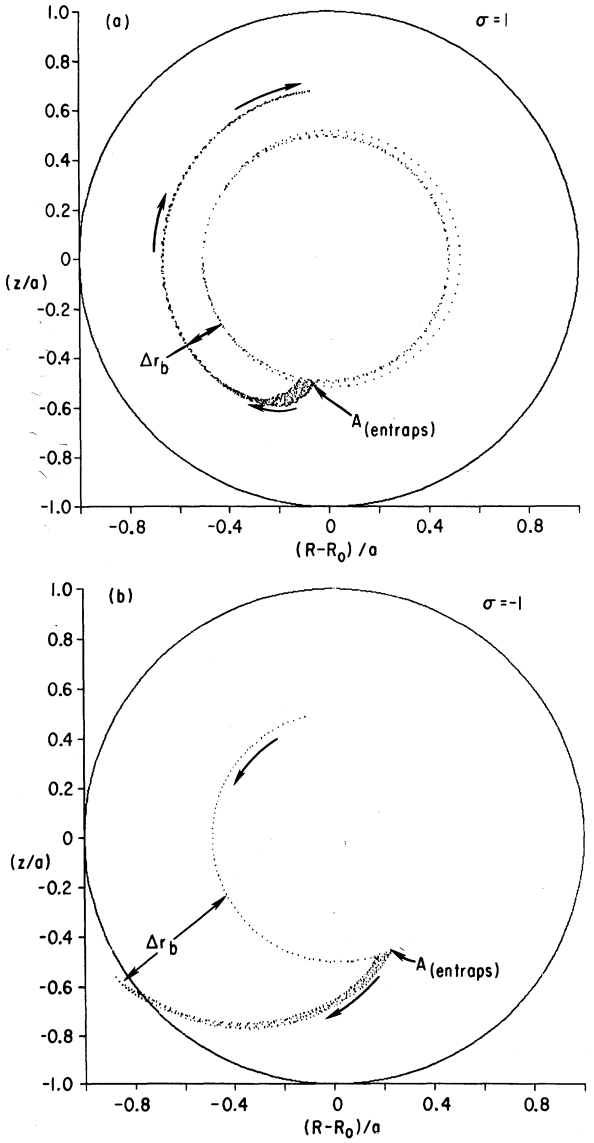

FIG. 3. Poloidal projections of orbits characteristic of those contributing dominantly to the transport at low ν, for (a) the $\sigma = 1$ and (b) the $\sigma = -1$ configurations. While the $\sigma = -1$ particle walks straight out of the device, once helically trapped, the $\sigma = 1$ particle has nearly omnigenous drifts, except for immediately after entrapping helically.

In Fig. 4 are shown the results of numerical runs done by using the guiding-center code with the Monte Carlo collision operator used in Refs. 3 and 6, for the $\sigma = 0, \pm 1$ configurations. As in Refs. 3 and 6, monoenergetic ensembles were used, started at initial radius $r/a = 0.5$, and randomly distributed in φ, θ, and pitch $\lambda \equiv v_{\parallel}/v$. For each value of collision frequency ν, an ensemble of eight particle orbits was used, which gave a standard deviation in the diffusion coefficients $D(\nu)$ so obtained of about 20%.

We quote parameters in terms of units where $a = m\,\Omega_0 = 1$, with m the particle mass and $\Omega_0 \equiv eB_0/mc$. In these units, a thermal ion with $m = 2.5$ u in a reactor-regime plasma ($T_i = 8$ keV, $n_i = 10^{14}$ cm^{-3}, $a = 2$ m, $B \simeq 5$ T) will have collisionality $\nu \simeq \nu_R \equiv 0.6\times 10^{-6}$ and energy $E = \frac{1}{2}(\rho/a)^2 \simeq 1.7\times 10^{-6}$. For these parameters a confinement time $\tau_E = a^2/4D$ of 1 sec corresponds to a diffusion coefficient $D = D/a^2\Omega_0 \simeq 1.25\times 10^{-9}$.

For the results in Fig. 4, the parameters taken were the same as in Fig. 1, along with $E = 10^{-6}$. One sees that $D(\sigma = 1)$ is down from $D(\sigma = 0)$ and $D(\sigma = -1)$ by one and two orders of magnitude, respectively. A run time $T = 2/\nu_R = 3.33\times 10^6$ was used for all orbits, independent of collision frequency ν. As pointed out in Ref. 3, for T less than the helical detrap time $\tau_h \equiv \epsilon_h/\nu$, the radial step Δr that a trapped particle takes then becomes limited by a *numerical* time T rather than *physical* time τ_h, leading to a spuriously low value for D at lower ν. To this we attribute the fact that $D(\sigma = 0)$ in Fig. 4 lies appreciably below the theoretical prediction. This argument assumes, however, that T is also smaller than the time τ_r that a trapped particle moves radially during the full period τ_θ of a superbanana orbit. This is justified for $\sigma = 0$, where $\tau_r \sim \tau_\theta$, but not for $\sigma = 1$, where $\tau_r < T < \tau_\theta$, because of the short, rapid radial step a trapped particle takes [Fig. 3(a)]. Therefore, one may expect the numerical values given for $D(\sigma = 1)$ to be closer to the real values, at lower ν, than for $D(\sigma = 0, -1)$. In fact, test runs for longer T at $\nu = 0.003$ showed a slow increase in D for $\sigma = 0$, and a decrease for $\sigma = 1$.

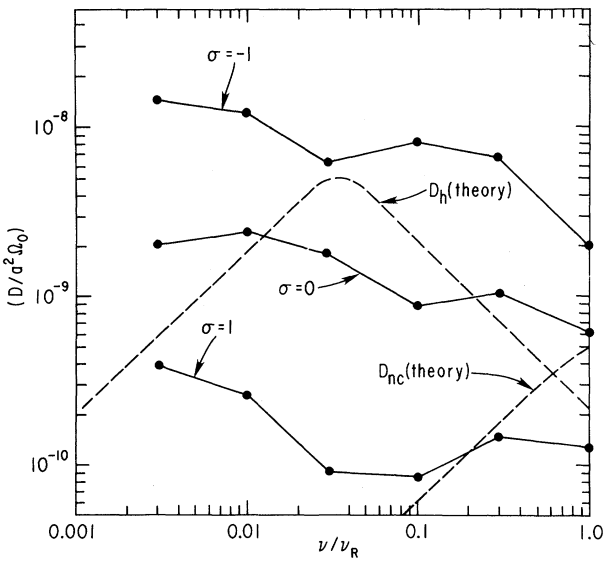

FIG. 4. Numerically obtained transport results, for the $\sigma = 0, \pm 1$ configurations, for parameters given in the text. The numerical points for each σ are connected by solid line segments. The dashed lines show the theoretical predictions for the helical or superbanana (D_h) and tokamak-neoclassical (D_{nc}) contributions to the transport.

The configuration studied here is idealized in a number of respects. Only pitch angle scattering was included since, by the standard arguments of neoclassical theory,[9] it dominates in the evaluation of the transport coefficients. Although only one particle energy was used in these studies one would expect the qualitative results to be independent of energy at a given collisionality. Also, one might question whether the favorable transport results are critically dependent upon the simple analytic model chosen for B, or the assumption of no shear. While further numerical work would be useful in ascertaining the sensitivity of the transport to departures from the present model of the magnetic field structure, the fact that Eqs. (3) and (4) seem adequate to understand the reduction in transport indicates that other configurations providing the same reduction in $\dot{r}$ for trapped particles will also display favorable confinement.

This work was supported by U. S. Department of Energy Contract No. DE-AC02-76-CH03073.

[a]Present address: Torsatron/Stellarator Laboratory, Department of Electrical and Computer Engineering, University of Wisconsin, Madison, Wisc. 53706.

[1]A. A. Galeev, R. Z. Sagdeev, H. P. Furth, and M. N. Rosenbluth, Phys. Rev. Lett. 22, 511 (1969).

[2]J. W. Connor and R. J. Hastie, Phys. Fluids 17, 114 (1974).

[3]H. E. Mynick, Princeton Plasma Physics Laboratory Report No. PPPL-1781, 1981 (to be published).

[4]F. Meyer and H. U. Schmidt, Z. Naturforsch. 13A, 1005 (1958).

[5]T. K. Chu, H. P. Furth, J. L. Johnson, C. Ludescher, and K. E. Weimer, private communications, and Princeton Plasma Physics Laboratory Report No. PPPL-1796, 1981 (unpublished).

[6]A. H. Boozer and G. Kuo-Petravic, Phys. Fluids 24, 851 (1981).

[7]R. E. Potok, P. A. Politzer, and L. M. Lidsky, Phys. Rev. Lett. 45, 1328 (1980).

[8]L. S. Hall and B. McNamara, Phys. Fluids 18, 552 (1975).

[9]M.N. Rosenbluth, R. D. Hazeltine, and F. L. Hinton, Phys. Fluids 15, 116 (1972).

Cool, High-Density Regime for Poloidal Divertors

M. Petravic, D. Post, D. Heifetz, and J. Schmidt

Plasma Physics Laboratory, Princeton University, Princeton, New Jersey 08544

(Received 29 June 1981)

Calculations have been performed which demonstrate the possibility of operating poloidal divertors at high densities and low temperatures. Ionization of recycling neutral gas near the divertor neutralizer plate amplifies the input particle flux thereby raising the plasma density and lowering the plasma temperature. Low-temperature, high-density operation should reduce the erosion rate of the divertor walls and plate, and ease the pumping requirements in future large tokamaks.

PACS numbers: 52.55.Gb

Early design work for proposed very large reactor-sized tokamak experiments, such as INTOR[1] and ETF,[2] has indicated that one of the chief difficulties of such devices is handling the particle and heat outfluxes of ~10^{23} particles/sec and ~100 MW. Applications of simple edge models[3] have led to the expectation that the edge would have a high temperature (500–2000 eV) and low density ($n_e \sim 10^{11}$–10^{12} particles/cm^3). For such conditions, the average energy per particle would be in the kiloelectronvolt range, resulting in erosion rates due to sputtering on the order of 25 cm/yr for materials such as iron.[4]

We have constructed a two-dimensional model for the steady-state plasma and neutral-gas flow in a poloidal divertor. The calculation is done in a Cartesian geometry with a rectangular divertor (Fig. 1) with plasma flowing into the divertor and striking the neutralizer plate near a pumping duct. We have used a set of flux-conserving fluid equations (1)–(4) to describe the plasma. Electron inertia was neglected and charge neutrality used to eliminate the electric field from (3) and (4):

$$\frac{\partial(nv_\xi)}{\partial\xi} = S_n(\xi, y) + \frac{\partial}{\partial y}\left(D\frac{\partial n}{\partial y}\right), \tag{1}$$

$$\frac{\partial}{\partial\xi}\left[n(mv_\xi^2 + T_i + T_e)\right] = S_p(\xi, y) + \frac{\partial}{\partial y}\left(mv_\xi D\frac{\partial n}{\partial y}\right), \tag{2}$$

$$\frac{\partial}{\partial\xi}\left[nv_\xi(\tfrac{5}{2}T_i + \tfrac{1}{2}mv_\xi^2)\right] = -v_\xi T_e\frac{\partial n}{\partial\xi} + S_{E_i}(\xi, y) + \frac{\partial}{\partial y}\left(\left[\tfrac{5}{2}T_i + \tfrac{1}{2}mv_\xi^2\right]D\frac{\partial n}{\partial y}\right), \tag{3}$$

$$\frac{\partial Q_e}{\partial\xi} = v_\xi T_e\frac{\partial n}{\partial\xi} + S_{E_e}(\xi, y) + \frac{\partial}{\partial y}\left(\left(\tfrac{3}{2}T_e\right)D\frac{\partial n}{\partial y}\right). \tag{4}$$

S_n, S_p, S_{E_i}, and S_{E_e} are the particle, momentum, and ion and electron energy source terms due to ionization, charge exchange, and radiation of the recycling neutral atoms. ξ is the coordinate along the field line, y is the coordinate perpendicular to the flux surface, and D is the cross-field diffusion coefficient.

The first three boundary conditions are the particle flux Γ and the electron and ion energy fluxes, $Q_e{}^0$, $Q_i{}^0$, at the divertor throat. The other two boundary conditions are the electron energy flux at the sheath boundary at the neutralizer plate, $Q_e{}^{sh} = \gamma 2T_e(nv_\xi)^{sh}$, and v_ξ, the plasma